PCCP

PAPER

View Article Online
View Journal

Cite this: DOI: 10.1039/c7cp02106b

The bouncing threshold in silica nanograin collisions

Maureen L. Nietiadi,[a] Philipp Umstätter,[a] Tiffany Tjong,[b] Yudi Rosandi,[b] Emmanuel N. Millán,[c] Eduardo M. Bringa[c] and Herbert M. Urbassek *[a]

Received 1st April 2017,
Accepted 30th May 2017

DOI: 10.1039/c7cp02106b

rsc.li/pccp

Using molecular dynamics simulations, we study collisions between amorphous silica nanoparticles. Our silica model contains uncontaminated surfaces, that is, the effect of surface hydroxylation or of adsorbed water layers is excluded. For central collisions, we characterize the boundary between sticking and bouncing collisions as a function of impact velocity and particle size and quantify the coefficient of restitution. We show that the traditional Johnson–Kendall–Roberts (JKR) model provides a valid description of the ingoing trajectory of two grains up to the moment of maximum compression. The distance of closest approach is slightly underestimated by the JKR model, due to the appearance of plasticity in the grains, which shows up in the form of localized shear transformation zones. The JKR model strongly underestimates the contact radius and the collision duration during the outgoing trajectory, evidencing that the breaking of covalent bonds during grain separation is not well described by this model. The adhesive neck formed between the two grains finally collapses while creating narrow filaments joining the grains, which eventually tear.

I. Introduction

Collisions of dust grains are ubiquitous in astrophysics, occurring in diverse places such as protoplanetary disks[1,2] and the dust tails of comets.[3,4] While the grain composition may vary, grains are typically classified as silica and ice grains. Dust particles have a complex structure; they are aggregates of small grains with sizes <1 μm.[5] The collision of dust particles is studied theoretically by means of granular-mechanics codes, which treat each grain as an entity with only a few degrees of freedom (translation, rotation).[6–8] In these codes, a variety of physical forces and torques must be taken into account, which describe the details of attractive, repulsive, dissipative and frictional interactions. These forces are often modeled by laws and parameters based on macroscopic concepts.[9] It remains unclear to what extent they apply to the collision of micro- or nanoscopic grains.

Molecular dynamics simulations may be used to test the assumptions underlying the granular-mechanics models. Such simulations have been carried out, in particular, for energetic grain collisions.[10,11] But they can also analyze the behavior at smaller collision velocities, and thus determine the sticking and bouncing behavior. Only a few such simulations have been reported, and mostly for generic interaction potentials such as the Lennard-Jones potential.[12–14] The sticking process is relevant for understanding the evolution of dust growth, since only sticking collisions will lead to grain agglomeration.[9]

An important exception is provided by the work of Sun *et al.*[15] who studied the collision of silica nanospheres (radii of 4 nm and below) using a non-reactive force field. This force field models the interatomic bonding and the van-der-Waals attraction between atoms, but does not allow for bonds to break and new bonds to form. This study showed that the collision of silica grains can be well described by the Johnson–Kendall–Roberts (JKR)[16] theory of adhesive contacts; in particular, the force-displacement curves and the contact radii are well reproduced.

However, more energetic collisions may lead to close encounters of the two grains where bonds may dissociate and new bonds may form. In particular, at the high pressures present in the compression phase, strong bonds may form between the two grains; such effects could not be considered in the previous study.[15]

In the present paper, we want to understand specifically the collisional behavior of silica grains. To this end, we use amorphous silica particles colliding at relatively small velocities, where their interaction is described by either sticking or bouncing. We compare the collision results with the available macroscopic JKR model. In addition, we characterize the changes induced in the material by the collision.

[a] *Fachbereich Physik und Forschungszentrum OPTIMAS, Universität Kaiserslautern, Erwin-Schrödinger-Straße, D-67663 Kaiserslautern, Germany. E-mail: urbassek@rhrk.uni-kl.de; Web: http://www.physik.uni-kl.de/urbassek/*

[b] *Department of Geophysics, Universitas Padjadjaran, Jatinangor, Sumedang 45363, Indonesia*

[c] *CONICET and Facultad de Ciencias Exactas y Naturales, Universidad Nacional de Cuyo, Mendoza, 5500, Argentina*

II. Method

A. Simulations

We use the potential devised by Munetoh *et al.*[17] to characterize the atomic interaction in silica. It is based on the bond-order scheme developed by Tersoff[18,19] to model the environment-dependent bonding of Si and O atoms. It was tested to describe the structural properties of various silica polymorphs, including the amorphous state, satisfactorily. Bonds are treated as covalent. We note that similar non-ionic potentials have been used previously to model the energetic impacts of silica clusters.[20–22]

We amorphized a large block of silica; in order to obtain an optimum structure we followed the procedure outlined in the study by Huff *et al.*[23] as number 2-VIII. Spheres with radii of R = 15, 20 and 25 nm – containing 0.96, 2.26, and 4.42 million atoms, respectively – were cut from this sample to be used as collision grains, and relaxed for 50 ps to the final temperature of 300 K before starting the collision.

The collision is started by duplicating the grain and shooting the two copies onto each other with a relative velocity v. Only central collisions are considered. At high enough velocities at which bouncing is observed, we calculate the relative center-of-mass velocity, v', of the two grains after the collision. The coefficient of restitution is then defined as

$$e = |v'|/v. \quad (1)$$

At small velocities, at which the two grains stick, it is $e = 0$.

The lowest velocity at which bouncing occurs is denoted as the bouncing velocity, v_b. In our simulations, we find a largest velocity without bouncing, $v^<$, and a lowest velocity with bouncing, $v^>$. We note that we did not find bouncing for smaller grains, $R < 15$ nm; we investigated grains with radii of 3.5, 5, and 10 nm for collision speeds between 200 and 3000 m s^{-1} and found sticking at smaller velocities followed by shattering (fragmentation) at larger velocities.

The molecular dynamics simulations are performed using the LAMMPS code.[24] Atomic snapshots are generated using OVITO.[25]

B. Materials parameters

Our a-SiO_2 sample exhibits a mass density of ρ = 2.25 g cm^{-3}, in good agreement with the experimental data (2.20 g cm^{-3}).[26,27] We determined the elastic properties by uniaxial and triaxial compressions; this gave us the bulk modulus of B = 49.9 GPa and the longitudinal modulus of c_{11} = 81.4 GPa. These values are larger than the experimental data of B = 36.8 GPa and c_{11} = 77.3 GPa;[27,28] note that the potential devised by Munetoh *et al.*[17] was not fitted to the elastic data of silica polymorphs; however, a recent study[29] reported that the elastic constants of α-quartz are reproduced within 10%. Amorphous samples are subject to inherent structural inhomogeneities; we created an ensemble of 10 further a-SiO_2 samples and estimated the uncertainty of our moduli to be ±5 GPa. From our results, we can calculate the Young's modulus E = 61.2 GPa and the Poisson ratio ν = 0.16 (experiment: E = 71.5 GPa, ν = 0.176). For further use, we note that the indentation modulus amounts to $E_{ind} = E/(1-\nu^2)$ = 67.1 GPa (experiment: E_{ind} = 73.8 GPa).

We determined the specific surface energy γ of our silica specimens by using a standard procedure.[30] The energy of a bulk silica specimen containing N molecules is given by NE_{coh} with a cohesive energy of E_{coh} = 19.64 eV per molecule. Let us denote the energy of a silica system containing a planar surface of area A by E_{tot}. Then, the specific surface energy is given by

$$\gamma = \frac{E_{tot} - NE_{coh}}{A}. \quad (2)$$

Our simulation gives γ = 1.43 ± 0.09 J m^{-2}. We note that this value is strongly affected by the details of the atomic configuration at the surface; a high number of dangling bonds increases this value, while the formation of siloxane (–Si–O–Si–) bridges would decrease it.[31]

The experimental data of the surface energy of silica show a large variety, γ = 0.02–2.5 J m^{-2} as reviewed in the recent compilation of Kimura *et al.*[32] This compilation also explains the reason for this variety by dividing the silica specimens into three groups according to the silica–water surface chemistry:[31] (i) silica covered by water multilayers has low surface energies, $\gamma \lesssim 0.1$ J m^{-2}; (ii) silica covered with a single water layer has $\gamma \lesssim 0.3$ J m^{-2}; (iii) naked silica has the highest surface energy, $\gamma > 0.3$ J m^{-2}. Our large value is in agreement with several measurements and calculations of the surface energy of pure silica in vacuum.[32]

III. Results

Fig. 1 illustrates the familiar result of a sticking collision below the bouncing threshold.[14,33] Upon contact, an adhesive neck is formed, Fig. 1(a), which increases while the two grains are driven deeper into each other. After the moment of largest compression, Fig. 1(b), the velocities are reversed, and the two grains increase their distance again. However, if the resulting adhesion is too large, the two grains will not separate but remain connected by the neck, Fig. 1(c). Oscillations are excited in the 2-grain system, Fig. 1(d). The final neck, Fig. 1(e), is smaller than the one at the moment of largest compression, but larger than the initial neck. This shows the hysteresis of the neck formation process. Note, furthermore, that around the final neck, several atoms have changed their places and moved from one grain to the other; this happened during the compression phases where the neck was at maximum width.

In the following sections, we shall investigate more energetic collisions which allow for grain separation.

A. Bouncing

Fig. 2 shows the coefficient of restitution for the collisions investigated. For each grain size investigated, bouncing occurs at velocities above the bouncing velocity, v_b. We note that we did not find bouncing for smaller grains, $R < 15$ nm.

The velocity dependence of the coefficient of restitution above v_b has been fitted to the law[34]

$$e_{JKR}(v) = \alpha\sqrt{1 - \left(\frac{v_b}{v}\right)^2}. \quad (3)$$

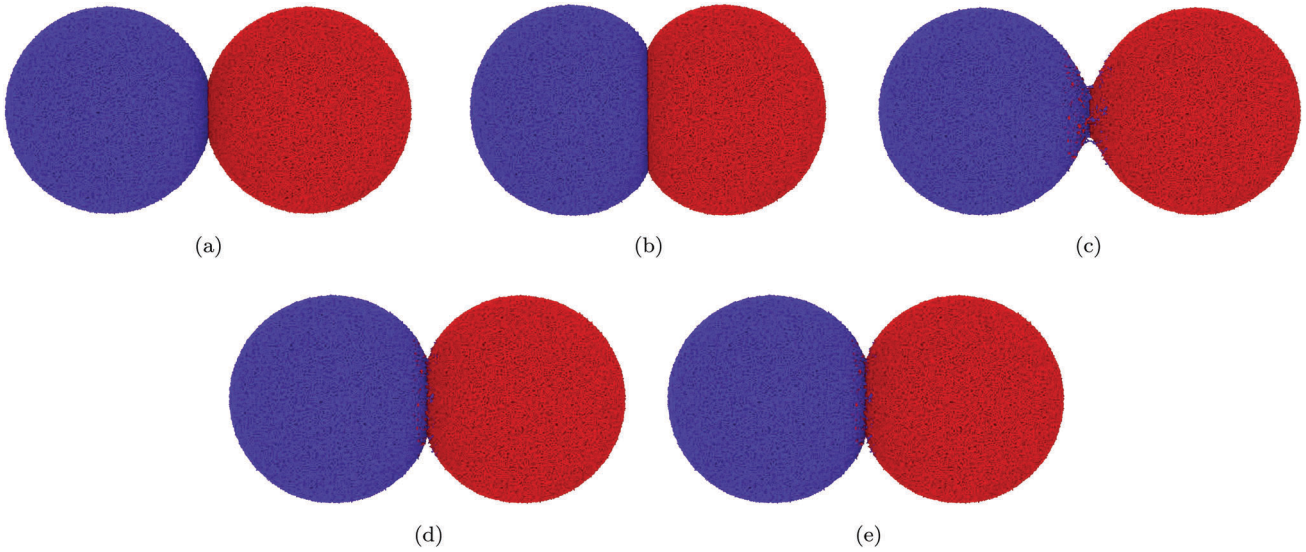

Fig. 1 Snapshots showing a sticking collision of two R = 20 nm grains at a velocity, v, = 450 m s^{-1}, slightly below the bouncing threshold at (a) the moment of contact, 3.75 ps, (b) the moment of deepest compression, 17.25 ps, (c) ensuing maximum elongation, 55.5 ps, (d) second compression, 82.5 ps, and (e) the final stage, 88.5 ps. Atoms are colored according to the original grain affiliation.

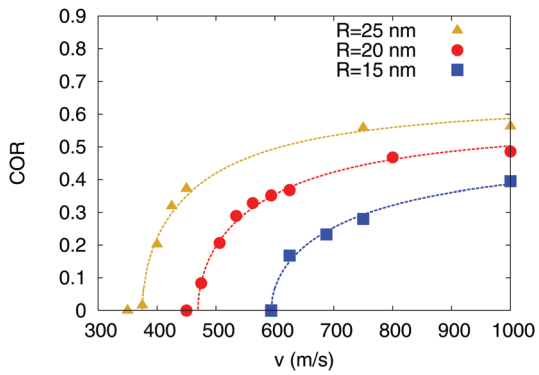

Fig. 2 Coefficient of restitution, COR, as a function of impact velocity, v. Symbols: simulation results. Lines: fit to eqn (3).

Such a law (with α = 1) can be justified theoretically for elastic collisions of adhesive spheres within the framework of the JKR theory of adhesive contacts.[16,33,35] The physical picture is as follows: when the two grains approach, they form an adhesive neck upon contact. During the collision, the kinetic collision energy is transformed into elastic energy, but released again to accelerate the two grains from each other. At low velocities, $v < v_b$, the kinetic energy of the two grains does not suffice to overcome the adhesive force of the neck; this scenario is compatible to our findings for sticking collisions, Fig. 1. At higher velocities, the neck is broken and the two grains separate. We add the constant factor α to account for energy dissipation during the collision, such as the excitation of oscillations in the 2-grain system, see Fig. 1.

Fig. 2 shows that the JKR estimate describes the coefficient of restitution quite well in the velocity regime beyond the bouncing velocity that we explored. We may obtain an estimate for v_b also from the fit to eqn (3); as shown by Table 1, it agrees well with our immediate simulation results. The values of α increase with grain size; this means that the influence of dissipation becomes relatively smaller for larger grains.

Theoretical estimates are available for the bouncing velocity from JKR theory. For two identical spheres, the estimate reads[33–35]

$$v_b = \left(\frac{C}{\rho}\right)^{1/2}\left(\frac{\gamma^5}{E_{ind}{}^2 R^5}\right)^{1/6}, \quad (4)$$

where ρ denotes the mass density. This formula features as basic ingredients the increase of the bouncing velocity with intergrain adhesion (as quantified by the surface energy γ) and the decrease with the grain elastic modulus (quantified by E_{ind}). Here, C is a materials independent constant which depends on the assumptions underlying the derivation. In a straightforward approach, the collision energy $(m^*/2)v_b{}^2$ (m^* is the reduced mass of the 2-grain system) is set equal to the adhesive work, *i.e.*, the line integral of the intergranular adhesive force. This gives C = 4.265.[34,35] Brilliantov *et al.*[33] pointed out that the work of adhesion is not clearly defined since the value of the initial contact area – that is when, after approaching, the two grains jump into contact – is not well-defined under the dynamic conditions of a collision; they therefore derived C = 0.30–5.25, but provided arguments for the larger value. They also pointed out that dissipative processes will increase v_b. This idea was taken up

Table 1 Bouncing velocity, v_b, and dissipation constant, α, as obtained from a fit of our simulation data, Fig. 2, for silica spheres of radius R to eqn (3). $v^<$ and $v^>$ denote the largest velocity at which the grains stick and the lowest velocity at which grains bounce, respectively, found in our simulations

R (nm)	$v^<$ (m s^{-1})	v_b (m s^{-1})	$v^>$ (m s^{-1})	α
15	594	594	625	0.48
20	450	469	475	0.57
25	350	375	375	0.63

by Krijt *et al.*[34] who set up a model including viscoelastic damping to study the effects on bouncing and the coefficient of restitution; they quantified the increase of v_b in terms of the viscoelastic parameters. In earlier work, Dominik and Tielens[9] argued that, in particular, dissipation by excitation of elastic waves will increase the value of v_b beyond that provided by the adhesive forces; they arrived at $C = 18.33$. Note that this paper corrects an error in their previous work.[36] Finally Kimura *et al.*[32] used $C = 57.9$ and demonstrated that this value provides a satisfactory agreement with experiments on the bouncing of small silica spheres (radii of 0.6 and 0.25 μm) from flat surfaces.[37] In the following sections, we shall use the latter value of $C = 57.9$.

In Fig. 3, we compare our simulation data with the prediction of eqn (4). Our results are compatible with the predicted $R^{-5/6}$ dependence on grain size. In detail, we observe that v_b decreases with R as a power law, $v_b \propto R^{-m}$, where $m = 0.88 \pm 0.05$. However, our data are a factor of about 3.4 too large. In view of the above discussion on the origin of that formula, we assume that energy dissipation during the collision as well as the nature of the adhesive neck – see the discussion on the intergranular filament formation in Section IIIB below – is responsible for this deviation.

Recently, the collision between two silica spheres was modeled by a non-reactive force field.[15] There, a tiny surface energy of $\gamma = 0.03$ J m^{-2} was determined, which was caused by the fact that only van-der-Waals forces were included between the two grains without the possibility of forming covalent bonds. We note that such small values are adequate for silica covered by multiple water layers. In correspondence with the small value of γ, the authors also observed bouncing at smaller velocities than in our study, even though they did not study systematically the bouncing transition.

B. Materials processes at the bouncing threshold

Fig. 4 illustrates the materials processes occurring at the bouncing threshold. We choose $R = 20$ nm grains colliding with 475 m s^{-1}. In this figure, atoms are colored according to the atomic shear strain they suffer. In technical terms, this quantity is the von-Mises invariant of the local shear strain tensor describing the atomic-level deformation with respect to a reference configuration, which is here taken as the initial grain configuration before collision.[38,39] In Fig. 4(a) we display the shear strain at the moment of largest compaction for a $R = 20$ nm collision. Unsurprisingly, the strongest sheared region is in the vicinity of the contact area. Note that the highest strains, surpassing $\varepsilon = 0.25$, appear in strongly localized small volumes, which indicate the occurrence of localized shear transformation zones (STZs). The relevance of STZs for the plasticity of amorphous materials has been known for long,[40–42] but here we demonstrate it in the formation of nanoplasticity in silica grain collisions. Note that plasticity in amorphous materials such as silica requires the breaking and reformation of bonds, in contrast to bond stretches or bends characterizing elastic deformation;[43] such processes cannot be modeled in non-reactive force fields. STZs may combine to form shear transformation bands, which soften the amorphous material since they allow shear and thus high energy dissipation. It is also in these regions that eventually cracks may form.

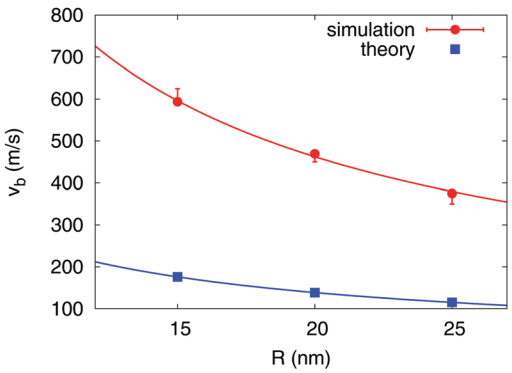

Fig. 3 Bouncing velocity, v_b, as a function of grain radius, R. Simulation data, Table 1, are compared to the prediction of JKR theory, eqn (4). The largest velocity at which the grains stick and the lowest velocity at which grains bounce are included in the simulation results in the form of error bars. The line connecting the simulation data presents a fit to a power law, $v_b \propto R^{-m}$, where $m = 0.883$.

The volumetric stress in the compaction zone stays below 10 GPa, and reaches such high values only in isolated atoms, but not in connected regions. It is known that stresses of this order of magnitude, such as those for instance reached under shock loading, may permanently transform the amorphous silica to a higher-density amorphous phase;[43] this behavior also occurs for the potential[17] used in the present study.[29] We note that such a densification renders silica more ductile due to the 5-fold Si coordination defects (bonded to 5 O neighbors) created in this process.[44] However, we did not observe such a phase transformation, presumably because the dense phase lasts only in the order of 20 ps. We note that the temperatures in the grain during collision rise in the contact zone, but the values remain below around 600 K.

We can estimate the pressures occurring during collision from $p = \rho v c_l$, where the longitudinal velocity of sound amounts to $c_l = 5900$ m s^{-1}.[27] This relationship originates from a simplification of the Hugoniot relationship[13] and is expected to work well under our conditions. At the bouncing velocity of the 20 nm grain, $v_b = 475$ m s^{-1}, this predicts $p = 6.3$ GPa, in fair agreement with our simulation results.

After the collision, Fig. 4(b), the strains have generally decreased. They are still considerable at the positions where the two grains met; these effects on the immediate contact zone will be discussed below. However, also in the grain interiors, close to the contact zone, strong shears remain; the clustering of the strongly sheared atoms gives evidence of the survival of the STZs. As a result, we found that the strong compression during the collision gave rise to defect formation in the grain interior – down to a depth corresponding to the radius of the contact area, *cf.* Fig. 4(a). After a multitude of impacts, such defects may lead to surface modifications of the grains resulting in a weakening of the mechanical properties of the grains and make them more sensitive to crack initiation and growth.

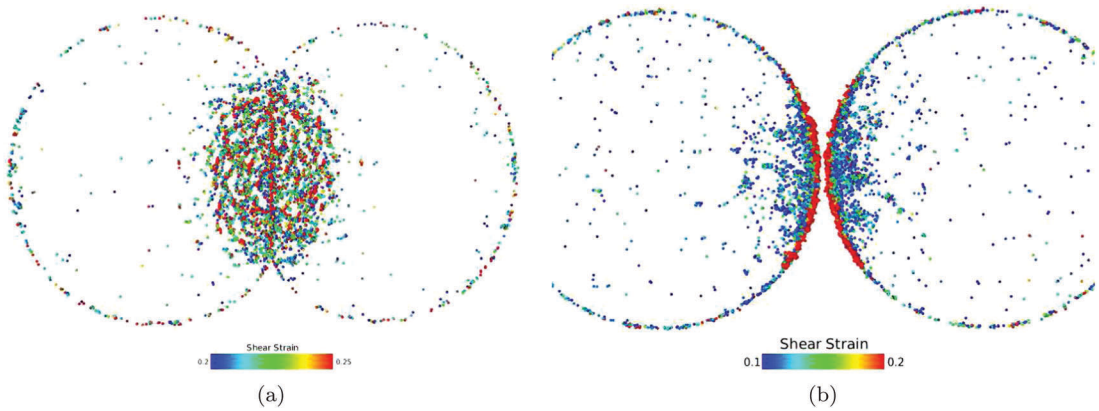

Fig. 4 Strained regions at the moment of largest compression (a) and after the collision (b) for the R = 20 nm grains colliding with v = 475 m s^{-1}. Only atoms experiencing a shear strain in excess of 0.2 (a) and 0.1 (b) are plotted, see the color bars.

We note that previous studies of crystalline grain collisions showed the occurrence of dislocation-based plasticity which – starting from the collision area – spanned the entire crystal.[13,14] We found here that the situation is different for amorphous grains, since the defect-induced plasticity remains concentrated in the vicinity of the collision area.

The surface of the contact zone has become strongly roughened on the atomic scale due to the high-pressure contact and separation that occurred. Such a roughening will be important in the space environment, since it will result in an enhanced surface area, with consequences for gas adsorption and possibly catalytic activity.[45]

In Fig. 5, we display the separation process of the two collided grains. The neck that has formed between the two grains due to grain adhesion is under strongly tensile stress; while the centers of the two grains move away from each other, the neck collapses to an array of thin filaments which are torn apart. Note how during the separation process the grain material is strongly mixed. These filaments may finally be of monoatomic thickness, occasionally branching. The silica structure is built on SiO_4 tetrahedra; when the contact neck is stretched, some Si–O bonds are broken, while the surviving bonds form the Si–O–Si–O filaments, as shown in Fig. 5, especially Fig. 5(c). Similar silica filaments have been observed in silica nanowires under tension,[46] where for small-diameter nanowires ductile fracture is observed in both experiments and simulations using a 3-body potential devised by Vashishta *et al.*,[47] while the two-body Beest–Kramer–Santen (BKS) potential[48] displays a different behavior. These figures illustrate the atomistic origins of the hysteresis in the neck formation and destruction process; while neck formation may be thought of as a quite generic (macroscopic) phenomenon that is well described by the surface energies of the two colliding grains, neck separation is best analyzed *via* atomistic simulations which allow taking the breaking of atomic bonds into account.

C. Comparison to JKR theory

The peculiarities of this neck separation process are also responsible for the quantitative increase of the bouncing velocity by a factor of 3.4 beyond the prediction of JKR theory, eqn (4). To demonstrate this effect, we plot in Fig. 6 the temporal evolution of the contact radius, a, between the two grains. It has been estimated by determining at each time the set of contact atoms; because of symmetry, these are situated in the mid-plane between the two grain centers. The largest distance of a contact atom to the line connecting the two centers of the grains then determines the radius of the contact area.

In the plot, we also include the prediction of JKR theory; it provides a connection between the overlap $\delta = 2R - d$ (d is the

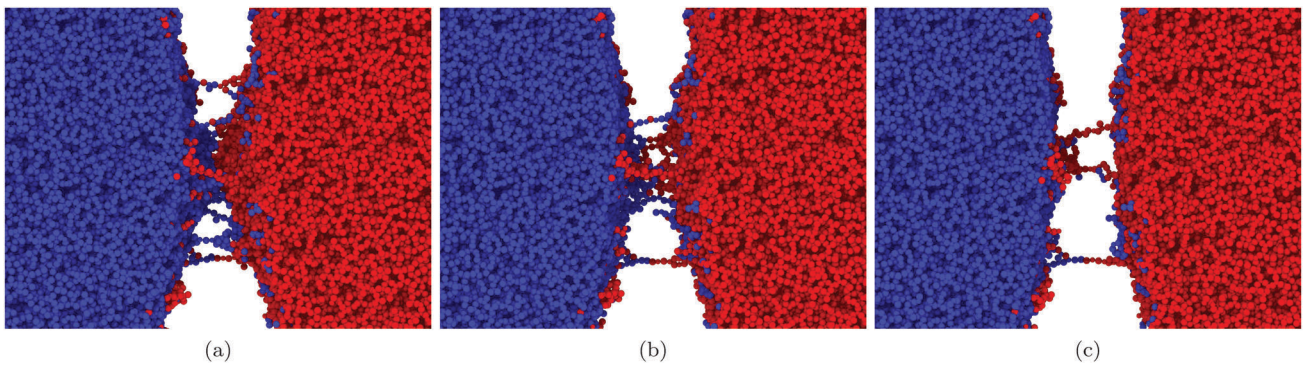

Fig. 5 Details of the separation of the two R = 20 nm grains (v = 475 m s^{-1}) at three consecutive times of (a) 56.25 ps, (b) 57 ps, and (c) 57.75 ps after impact. Atoms are colored according to the original grain affiliation. Si atoms are drawn slightly larger than O atoms.

distance between the centers of the two grains) and the contact radius a. The center of each grain is identified by the position of its central atom; since strains in the grain centers are negligible, see Fig. 4, the identity of the central atoms is preserved during the collision. For two equal spheres, JKR predicts[33,49]

$$\delta = \frac{2a_{\mathrm{JKR}}{}^2}{R} - \sqrt{8\pi\frac{\gamma a_{\mathrm{JKR}}}{E_{\mathrm{ind}}}}. \quad (5)$$

We use this equation to determine a_{JKR} from the simulation data of $\delta(t)$.

For orientation, we note that the contact radius $a_{\mathrm{JKR}}^{\mathrm{equ}}$ of two unforced spheres, *i.e.*, when no external force is acting, amounts to

$$a_{\mathrm{JKR}}^{\mathrm{equ}} = \left(\frac{9\pi}{2}\frac{\gamma R^2}{E_{\mathrm{ind}}}\right)^{1/3}. \quad (6)$$

For our system, it is $a_{\mathrm{JKR}}^{\mathrm{equ}} = 4.94$ nm. At contact, $\delta = 0$, the radius is $a_{\mathrm{JKR}}^{0} = (4/9)^{1/3} a_{\mathrm{JKR}}^{\mathrm{equ}} = 3.77$ nm. JKR theory also predicts that a contact becomes unstable if the contact radius falls below $(1/4)^{1/3} a_{\mathrm{JKR}}^{\mathrm{equ}} = 3.11$ nm.

In Fig. 6, the times when the centers of the two grains are at a distance of $2R$ (zero overlap) are marked. During the incoming trajectory, JKR reproduces well our simulation results. However, the maximum contact radius is slightly larger than the JKR prediction; we assume that this is due to the plastic deformation occurring during maximum compression, see Section IIIB above; this is not included in the elastic JKR theory. The largest differences occur in the outgoing trajectory; there, the simulation results are considerably larger than the prediction. At the time, when the two grains separate – $\delta = 0$, at 37.5 ps – the contact radius is still 7.50 nm, far above the JKR value of 3.77 nm. The actual separation takes another 18.75 ps until the contact radius has decreased to zero, *i.e.*, until the filamented neck has completely torn. Note during the separation process the extended period of time from around 40–50 ps, where the contact radius stays constant; this is the time when the formation of filaments prevents the separation of the two grains. We conclude from this discussion that the deviation from JKR theory occurs, in particular, during the separation stage; while many bonds have been created during the compression phase, the breaking of these bonds leads to considerable deviations from the continuum picture provided by JKR theory.

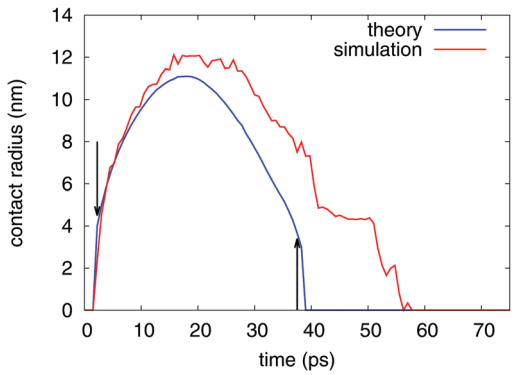

Fig. 6 Temporal evolution of the contact radius of two $R = 20$ nm grains colliding with $v = 475$ m s^{-1}. The simulation results are compared to the estimate of JKR theory, eqn (5). The arrows mark the times when the two grains are at a distance of $d = 2R$ (overlap $\delta = 0$), $t = 2.25$ and $t = 37.5$ ps. The contact ends at $t = 56.25$ ps in the simulations.

Besides JKR theory, other continuum theories have been set up to describe adhesive elastic contacts. Among them, the most widely known is the Derjaguin–Muller–Toporov (DMT) theory.[50] The DMT theory is assumed to describe stiff and small spheres, while JKR theory applies to compliant large spheres.[49,51] DMT theory is based on the idea that adhesive forces are only active in an annular ring around the contact zone, which is described by Hertz theory; however, this scenario is clearly ruled out by our MD observation of strong covalent forces acting in the contact zone itself. Also quantitatively, DMT theory does not describe our observations. Indeed, the DMT contact radius is smaller than that calculated by JKR theory;[49] for instance in the load-free case, $a_{\mathrm{DMT}}^{\mathrm{equ}}$ is a factor $(1/3)^{1/3} = 0.69$ of $a_{\mathrm{JKR}}^{\mathrm{equ}}$, eqn (6). In view of the good description of our simulated contact radius by JKR theory during the ingoing trajectory, Fig. 6, the small values predicted by DMT theory are clearly not adequate to describe our data.

IV. Summary

We studied the collision of silica nanograins using atomistic simulations. We focus on bare silica whose surface is not chemically modified by adsorbates, and which can hence form strong bonds between the colliding grains. This is in contrast to studies which assume the silica surfaces to be passivated by hydroxylation or by the adsorption of water layers; such surfaces are only able to exert weak van-der-Waals forces on each other, besides electrostatic interactions that may have length scales of up to 1 μm.[52] The conditions investigated by us may for instance prevail for dust collisions in the vicinity of a star, where temperatures are so high (above around 190 °C) that all water layers have desorbed.[31]

We note that high temperatures might influence the dynamics of grain–grain collisions; further simulations would be required to understand quantitatively the influence of elevated temperatures on the bouncing velocity. Elastic properties only change around 10–15% up to near 1500 K,[53,54] and also show little changes[55,56] at and beyond the glass temperature (1475 K[57]). Significant changes would only occur closer to the melting point of silica (1986 K [ref. 58, p. 4-84]).

The available experiments on collisions of silica spheres are performed in an environment which provides silica with a hydroxylated surface, in which dangling bonds are passivated, or even with one or multiple adsorbed water layers, see the extended discussion in the review article by Kimura *et al.*[32] Such a surface leads to a small surface energy in the range of $\gamma = 0.02$–0.1 J m^{-2}, and consequently to bouncing velocities that are a factor of one to two orders of magnitude smaller than those found for bare silica surfaces in the present study.

Concentrating on processes occurring around the bouncing threshold, we found the following.

(1) The traditional JKR model provides a good model to describe the coefficient of restitution in the vicinity of the bouncing transition. However, dissipation of energy prevents the coefficient of restitution to reach the value of 1 at high velocities and has to be included *ad hoc* in the model.

(2) The JKR model also provides an estimate of the magnitude of the bouncing velocity. It is in qualitative agreement with the results obtained from atomistic simulations. In particular, the $R^{-5/6}$ dependence of the bouncing velocity on grain size predicted by the model is followed by our results.

(3) Quantitatively, our results are a factor of around 3.4 larger than the estimate. We argue that the peculiarities of the breaking of the adhesive neck is responsible for this deviation, which are outside the continuum JKR model.

(4) JKR theory describes quantitatively well the ingoing trajectory of the two colliding grains. Deviations occur at maximum compression and, most pronouncedly, in the outgoing trajectory.

(5) During the high-pressure compression phase of the collision, nanoplasticity is generated in the amorphous grains. This leads to a slightly larger grain overlap at maximum compression than that predicted by the elastic JKR model. In addition, we see evidence for the formation of STZs that are confined to the collision zone, extending around one contact radius towards the grain interior. Multiple collisions might then lead to the formation of shear bands, thus inducing softening or cracking of the grains.

(6) This behavior is opposed to the nanoplasticity observed in crystalline grains, where grain-spanning dislocations are created such that the effect of a collision does not remain localized within the collision region.

(7) Another consequence of the collision is the roughening of the surface in the vicinity of the contact area, which is created during the grain separation stage. Such a roughening may be important in astrophysical contexts, since it will result in an enhanced surface area, with consequences for gas adsorption and possibly catalytic activity.

(8) Neck separation is best analyzed *via* atomistic simulations which allow taking the breaking of atomic bonds into account. In the case of silica grains studied here, the neck collapses upon the creation of filaments joining the grains, which ultimately tear.

These simulations neglect the role of possible net charging of the silica nanoparticles. Electrostatic forces and charge exchange during collisions might affect the contact radius and possibly increase even further the bouncing velocity. There are schemes for charge exchange in classical simulations,[59] but they are extremely expensive computationally compared to the Tersoff-type 3-body potential used here. Future simulations of colliding water-covered silica clusters would likely entail considering such electrostatic effects.

Other continuum models like DMT theory also fail to describe the complex bonding in silica.

The formation of filaments upon collisions seen in silica grain collisions in the present study might be a general feature also for other materials like silicon carbide, or carbon, where similar filaments have been seen in graphitic allotropes under tension,[60,61] and, in particular, under diamond–grain collisions.[62]

Acknowledgements

EM and EMB acknowledge support from SeCTyP-UNCuyo Grant No. M003, from ANPCyT Grant No. PICT-2014-0696, and from CONICET. HMU and PU are grateful for support by the Deutsche Forschungsgemeinschaft *via* the Sonderforschungsbereich 926.

References

1 J. Blum, *Res. Astron. Astrophys.*, 2010, **10**, 1199.
2 T. Birnstiel, M. Fang and A. Johansen, *Space Sci. Rev.*, 2016, **205**, 41.
3 M. S. Bentley, R. Schmied, T. Mannel, K. Torkar, H. Jeszenszky, J. Romstedt, A.-C. Levasseur-Regourd, I. Weber, E. K. Jessberger and P. Ehrenfreund, *et al.*, *Nature*, 2016, **537**, 73.
4 Y. Langevin, M. Hilchenbach, N. Ligier, S. Merouane, K. Hornung, C. Engrand, R. Schulz, J. Kissel, J. Rynö and P. Eng, *Icarus*, 2016, **271**, 76.
5 B. T. Draine, *Annu. Rev. Astron. Astrophys.*, 2003, **41**, 241.
6 D. Paszun and C. Dominik, *Astron. Astrophys.*, 2009, **507**, 1023.
7 K. Wada, H. Tanaka, T. Suyama, H. Kimura and T. Yamamoto, *Astrophys. J.*, 2007, **661**, 320.
8 C. Ringl, E. M. Bringa, D. S. Bertoldi and H. M. Urbassek, *Astrophys. J.*, 2012, **752**, 151.
9 C. Dominik and A. G. G. M. Tielens, *Astrophys. J.*, 1997, **480**, 647.
10 M. Kalweit and D. Drikakis, *Phys. Rev. B: Condens. Matter Mater. Phys.*, 2006, **74**, 235415.
11 N. Ohnishi, E. M. Bringa, B. A. Remington, G. Gilmer, R. Minich, Y. Yamaguchi and A. G. G. M. Tielens, *J. Phys.: Conf. Ser.*, 2008, **112**, 042017.
12 H. Tanaka, K. Wada, T. Suyama and S. Okuzumi, *Prog. Theor. Phys. Suppl.*, 2012, **195**, 101.
13 E. N. Millán, D. R. Tramontina, H. M. Urbassek and E. M. Bringa, *Phys. Chem. Chem. Phys.*, 2016, **18**, 3423.
14 E. N. Millán, D. R. Tramontina, H. M. Urbassek and E. M. Bringa, *Phys. Rev. E*, 2016, **93**, 063004.
15 W. Sun, Q. Zeng, A. Yu and K. Kendall, *Langmuir*, 2013, **29**, 7825.
16 K. L. Johnson, K. Kendall and A. D. Roberts, *Proc. R. Soc. London, Ser. A*, 1971, **324**, 301.
17 S. Munetoh, T. Motooka, K. Moriguchi and A. Shintani, *Comput. Mater. Sci.*, 2007, **39**, 334.
18 J. Tersoff, *Phys. Rev. B: Condens. Matter Mater. Phys.*, 1988, **38**, 9902.
19 J. Tersoff, *Phys. Rev. B: Condens. Matter Mater. Phys.*, 1989, **39**, 5566.
20 J. Samela, K. Nordlund, J. Keinonen, V. N. Popok and E. E. B. Campbell, *Eur. Phys. J. D*, 2007, **43**, 181.
21 J. Samela and K. Nordlund, *Phys. Rev. B: Condens. Matter Mater. Phys.*, 2010, **81**, 054108.
22 E. Holmström, J. Samela and K. Nordlund, *Europhys. Lett.*, 2011, **96**, 16005.
23 N. T. Huff, E. Demiralp, T. Cagin and W. A. Goddard III, *J. Non-Cryst. Solids*, 1999, **253**, 133.
24 S. Plimpton, *J. Comput. Phys.*, 1995, **117**, 1, http://lammps.sandia.gov/.

25 A. Stukowski, *Modell. Simul. Mater. Sci. Eng.*, 2010, **18**, 015012, http://www.ovito.org/.
26 P. Hudon, I.-H. Jung and D. R. Baker, *Phys. Earth Planet. Sci. Int.*, 2002, **130**, 159.
27 T. Deschamps, J. Margueritat, C. Martinet, A. Mermet and B. Champagnon, *Sci. Rep.*, 2014, **4**, 7193.
28 W. Pabst and E. Gregorova, *Ceram.-Silik.*, 2013, **57**, 167.
29 J. Wang, A. M. Rajendran and A. M. Dongare, *J. Mater. Sci.*, 2015, **50**, 8128.
30 D. Wolf, *Surf. Sci.*, 1990, **226**, 389.
31 L. Zhuravlev, *Colloids Surf., A*, 2000, **173**, 1.
32 H. Kimura, K. Wada, H. Senshu and H. Kobayashi, *Astrophys. J.*, 2015, **812**, 67.
33 N. V. Brilliantov, N. Albers, F. Spahn and T. Pöschel, *Phys. Rev. E: Stat., Nonlinear, Soft Matter Phys.*, 2007, **76**, 051302.
34 S. Krijt, C. Güttler, D. Heißelmann, C. Dominik and A. G. G. M. Tielens, *J. Phys. D*, 2013, **46**, 435303.
35 C. Thornton and Z. Ning, *Powder Technol.*, 1998, **99**, 154.
36 A. Chokshi, A. G. G. M. Tielens and D. Hollenbach, *Astrophys. J.*, 1993, **407**, 806.
37 T. Poppe, J. Blum and T. Henning, *Astrophys. J.*, 2000, **533**, 454.
38 A. Stukowski, 2010 ff, https://www.ovito.org/manual/.
39 A. Stukowski and A. Arsenlis, *Modell. Simul. Mater. Sci. Eng.*, 2012, **20**, 035012.
40 M. L. Falk and J. S. Langer, *Phys. Rev. E: Stat. Phys., Plasmas, Fluids, Relat. Interdiscip. Top.*, 1998, **57**, 7192.
41 C. A. Schuh and A. C. Lund, *Nat. Mater.*, 2003, **2**, 449.
42 P. Y. Huang, S. Kurasch, J. S. Alden, A. Shekhawat, A. A. Alemi, P. L. McEuen, J. P. Sethna, U. Kaiser and D. A. Muller, *Science*, 2013, **342**, 224.
43 L. P. Dávila, M.-J. Caturla, A. Kubota, B. Sadigh, T. Daz de la Rubia, J. F. Shackelford, S. H. Risbud and S. H. Garofalini, *Phys. Rev. Lett.*, 2003, **91**, 205501.
44 F. Yuan and L. Huang, *Sci. Rep.*, 2014, **4**, 5035.
45 A. Li and J. M. Greenberg, in *Solid state astrochemistry*, ed. V. Pirronello, J. Krelowski and G. Manicò, NATO Science Series II: Mathematics, Physics and Chemistry, Kluwer Academic Publishers, Dordrecht, 2000, vol. 120, p. 37.
46 J. Luo, J. Wang, E. Bitzek, J. Y. Huang, H. Zheng, L. Tong, Q. Yang, J. Li and S. X. Mao, *Nano Lett.*, 2016, **16**, 105.
47 P. Vashishta, R. K. Kalia, J. P. Rino and I. Ebbsjo, *Phys. Rev. B: Condens. Matter Mater. Phys.*, 1990, **41**, 12197.
48 B. W. H. van Beest, G. J. Kramer and R. A. van Santen, *Phys. Rev. Lett.*, 1990, **64**, 1955.
49 D. Maugis, *Contact, adhesion and rupture of elastic solids*, Springer, Berlin, 2000.
50 B. V. Derjaguin, V. M. Muller and Y. P. Toporov, *J. Colloid Interface Sci.*, 1975, **53**, 314.
51 J. A. Greenwood, *Proc. R. Soc. London, Ser. A*, 1997, **453**, 1277.
52 E. J. R. Parteli, J. Schmidt, C. Blümel, K.-E. Wirth, W. Peukert and T. Pöschel, *Sci. Rep.*, 2014, **4**, 6227.
53 S. Spinner, *J. Am. Ceram. Soc.*, 1962, **45**, 394.
54 B. D. Beake and J. F. Smith, *Philos. Mag. A*, 2002, **82**, 2179.
55 J. A. Bucaro and H. D. Dardy, *J. Appl. Phys.*, 1974, **45**, 5324.
56 M. Fukuhara and A. Sanpei, *Jpn. J. Appl. Phys.*, 1994, **33**, 2890.
57 M. I. Ojovan, *Adv. Condens. Matter Phys.*, 2008, **2008**, 817829.
58 *CRC Handbook of Chemistry and Physics*, ed. W. M. Haynes, CRC Press, Boca Raton, FL, 97th edn, 2016.
59 Y. K. Shin, T.-R. Shan, T. Liang, M. J. Noordhoek, S. B. Sinnott, A. C. van Duin and S. R. Phillpot, *MRS Bull.*, 2012, **37**, 504.
60 K. M. Liew, X. Q. He and C. H. Wong, *Acta Mater.*, 2004, **52**, 2521.
61 H. Zhang, Z. Duan, X. Zhang, C. Liu, J. Zhang and J. Zhao, *Phys. Chem. Chem. Phys.*, 2013, **15**, 11794.
62 D. F. Johnson, J. M. Mullin and W. D. Mattson, *J. Phys. Chem. C*, 2017, **121**, 1140.

